Face Clustering: Representation and Pairwise Constraints

Yichun Shi, *Student Member, IEEE,* Charles Otto, *Member, IEEE,* and Anil K. Jain, *Fellow, IEEE*

***Abstract*—Clustering face images according to their identity has two important applications: (i) grouping a collection of face images when no external labels are associated with images, and (ii) indexing for efficient large scale face retrieval. The clustering problem is composed of two key parts: face representation and choice of similarity for grouping faces. We first propose a representation based on ResNet, which has been shown to perform very well in image classification problems. Given this representation, we design a clustering algorithm, Conditional Pairwise Clustering (ConPaC), which directly estimates the adjacency matrix only based on the similarity between face images. This allows a dynamic selection of number of clusters and retains pairwise similarity between faces. ConPaC formulates the clustering problem as a Conditional Random Field (CRF) model and uses Loopy Belief Propagation to find an approximate solution for maximizing the posterior probability of the adjacency matrix. Experimental results on two benchmark face datasets (LFW and IJB-B) show that ConPaC outperforms well known clustering algorithms such as k-means, spectral clustering and approximate rank-order. Additionally, our algorithm can naturally incorporate pairwise constraints to obtain a semi-supervised version that leads to improved clustering performance. We also propose an k-NN variant of ConPaC, which has a linear time complexity given a k-NN graph, suitable for large datasets.**

***Index Terms*—face clustering, face representation, Conditional Random Fields, pairwise constraints, semi-supervised clustering.**

I. Introduction

CAMERAS are everywhere, embedded in billions of smart phones and hundreds of millions of surveillance systems. Surveillance cameras, in particular, are a popular security mechanism employed by government agencies and businesses alike. This has resulted in the capture of suspect facial images in high profile cases such as the 2013 Boston Marathon Bombing [1]. But, getting to the point of locating suspects' facial images typically requires manual processing of large volumes of images and videos of an event. The need for automatic processing of still images and videos to assist in forensic investigations has motivated prior work on clustering large collections of faces by identity [2].

In surveillance applications, the quality of available face images is typically quite low compared to face images in some of the public domain datasets such as the Labeled Faces in the Wild (LFW) [3]. The IARPA Janus project is pushing the boundaries of unconstrained face recognition and has released a dataset, NIST IJB-B [4][1], where many of the faces cannot be detected by off-the-shelf face detectors [6]. The face recognition problem posed by the Janus benchmark data may therefore be closer to that encountered in forensic applications. We attempt to handle this more difficult category of faces by: (i) improving the face representation (through the use of large training sets, and state-of-the-art deep network architectures), (ii) developing an effective face clustering algorithm to automatically group faces in images and videos, and (iii) by incorporating user feedback during the clustering process via a semi-supervised extension of the proposed clustering algorithm.

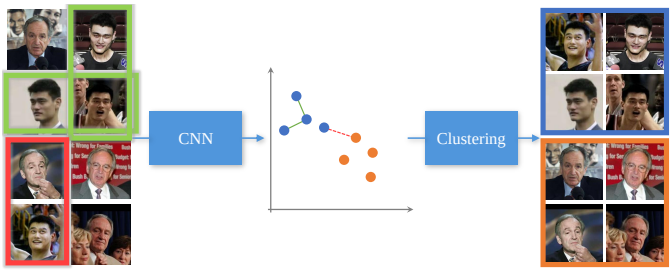

Fig. 1: Face clustering workflow. A deep neural network is trained to generate the representations for aligned face images. Given the representation and a similarity measure, goal of clustering is to group these unlabeled face images according to their identity. In the semi-supervised scenario, the pairwise constraints are also provided along with the unlabeled data. The red line here indicates a cannot-link pair and green lines indicate must-link pairs.

To develop a representation for face clustering, we leverage two public domain datasets: CASIA-Webface [7] and VGG-Face [8]. In terms of network architecture, we adopt deep residual networks, which have resulted in better performance than VGG-architecture on the ImageNet benchmark [9], and improved results over the architecture proposed in [7] on the BLUFR protocol.

Given a representation, we propose a face clustering method, called *Conditional Pairwise Clustering (ConPaC)* to group the face collection according to their hidden class (subject identity) using the pairwise similarity between face images. No additional information, including the true number of identities (clusters) is assumed. Instead of learning new similarity measures or representations and feeding them to a standard partitional or hierarchical clustering method, Conditional Pairwise Clustering directly treats the adjacency between all pairs of faces as the variables to predict and look for a solution that maximizes the joint posterior probability of these variables given their corresponding pairwise similarity. To model this conditional distribution, we propose a triplet consistency constraint which reveals such a dependency be-

Y. Shi and A. K. Jain are with the Department of Computer Science and Engineering, Michigan State University, East Lansing, MI, 48824. E-mail: shiyichu@msu.edu, jain@cse.msu.edu

C. Otto is with Noblis, Reston, VA. E-mail: ottochar@gmail.com

[1]There is also an earlier version with smaller number of images, called IJB-A released in 2015 [5]

tween the output variables that a valid adjacency matrix must be transitive to represent a partitional clustering. That means any two adjacent points should share exactly the same adjacent neighbors. The proposed model can dynamically determine the number of clusters, and also retain the similarity information. In particular, we model the problem as a Conditional Random Field (CRF) and employ Loopy Belief Propagation to arrive at a valid adjacency matrix. This model is easily extended to the semi-supervised case by accepting a set of pairwise constraints (either must-link, or cannot-link assignments) on the similarity matrix.

We perceive the following contributions in this work: (i) experimental evaluation of Deep Residual Networks for face representation and recognition, (ii) a clustering algorithm (ConPaC) based on direct estimation of an adjacency matrix derived from pairwise similarity between faces using the learned representation in (i), (iii) face clustering evaluation on two unconstrained face datasets: LFW and IJB-B, (iv) an extension of the proposed method to semi-supervised face clustering, and (v) an approximate k-NN variant of the algorithm for efficient clustering of millions of face images.

II. Background

A. Face Representation

Face images have been traditionally represented by appearance models or local descriptors [10] [11] [12] [13]. But after the success of Deep Neural Networks (DNN) in object recognition [14], a number of DNN based methods have been proposed for face representation and recognition. The DeepFace [15] method trained a CNN on a dataset of four million facial images belonging to more than 4,000 identities. The training is based on minimizing classification error with the output of the last hidden layer before classification layer taken as the face representation. DeepFace significantly surpassed the traditional methods in face recognition, especially for unconstrained face images. Sun et al. extended the work of DeepFace in their DeepId series [16] [17] [18] [19]. They proposed to use multiple CNNs with joint Bayesian framework [20] and added supervision to early convolutional layers. Schroff et al. [21], in their FaceNet work, abandoned the classification layer and instead introduced the triplet loss to directly learn an embedding space where feature vectors of different identities could be separated with Euclidean distance.

B. Face Clustering

Cluster analysis is an important topic widely studied in pattern recognition, statistics and machine learning [22]. It is useful for exploratory analysis by a preliminary grouping of a collection of unlabeled data. Due to potentially large and unknown number of identities in many large scale face collections, it is useful to tag the face images by clustering. Otto et al. [2] provided a brief review of face clustering. Most of the previous studies [23] [24] [25] [26] [27] focused on learning a good similarity matrix using the facial representations and then fed the matrix to a standard clustering algorithms such as spectral clustering to find clusters. However, the representations they used restrict the reliability of the similarity matrix. We use deep representations to attain more robust face representation and hence pairwise similarity and design a new clustering algorithm which could better retain the similarity information. The approximate rank-order clustering proposed by Otto et al. [28] [2] did use deep representation and is both efficient and effective for face clustering, but it is not capable of incorporating pairwise constraints for semi-supervised clustering. Further, we evaluate several networks and training protocols to obtain a better face representation than in [28] [2]. In [29], Nech et al. used face clustering to help label face images and built MF2 face dataset.

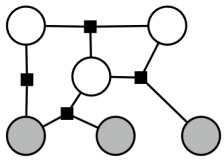

Fig. 2: An example factor graph of a general CRF model. Here, the filled nodes are input nodes and the white nodes are output nodes. Each factor (square) represents a potential function on a clique, encoding the contraints between nodes. There are constraints either between input and output or between output nodes. The figure is taken from [42].

C. Semi-supervised Clustering

Given the difficult nature of data clustering (choice of feature representation, similarity measure, distance and unknown number of clusters), one approach to improve clustering performance is to incorporate side-information. One common form of side-information is pairwise constraints, indicating that a pair of data points either must be placed in the same cluster (a "must-link" constraint), or they cannot be placed in the same cluster (a "cannot-link" constraint), as shown in Figure 1. Wagstaff et al. [30] first incorporated the pairwise constraints into k-means algorithm by forcing the hard cluster assignment to satisfy the constraints and showed that user-specified constraints could help to improve clustering results. Xing et al. [31] proposed to learn a Mahalanobis distance metric from the given constraints before applying k-means. Basu et al. [32] designed a probabilistic model for semi-supervised clustering with Hidden Markov Random Fields (HMRFs) and used EM algorithm to optimize the parameters. Research has also been conducted on incorporating pairwise constraints into hierarchical clustering [33] and spectral clustering [34] [35]. For a review of semi-supervised clustering, readers are referred to [36].

D. Conditional Random Fields (CRFs)

Conditional Random Fields (CRFs) are a type of undirected probabilistic graphical models first proposed by Lafferty et al. for predicting labels of sequential data [37] and later introduced to computer vision to model images [38] [39] [40]. The difference between CRFs and traditional Hidden Marcov Models (HMMs) [41] lies in that CRF is a discriminant model which directly models the conditional distribution $p(Y|X)$ rather than joint distribution $p(Y, X)$ and predicts the labels

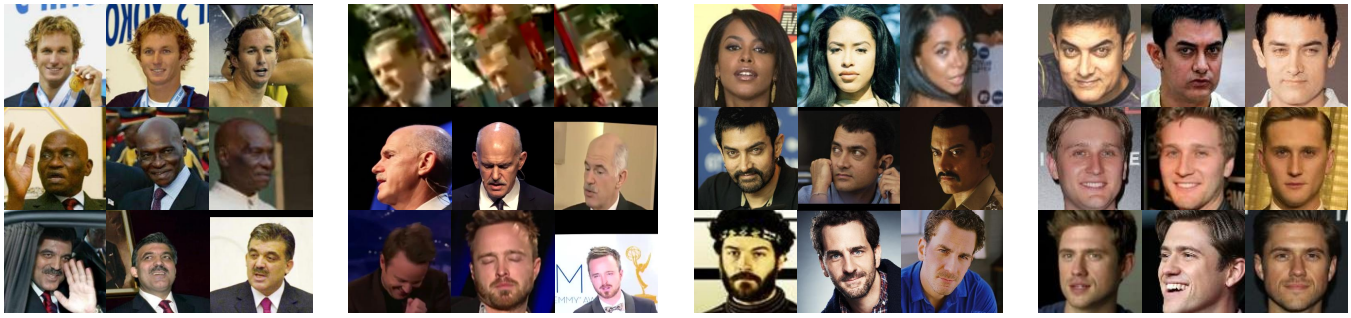

(a) (b) (c) (d)

Fig. 3: Example face images from (a) LFW, (b) IJB-B, (c) CASIA-webface, and (d) VGG datasets.

Y by maximizing the posterior probability. Generally, a CRF can be formulated as:

$$p(Y|X) = \frac{1}{Z} \prod_{C_p \in C} \prod_{\psi_c \in C_p} \psi_c(X_c, Y_c; \theta_p), \quad (1)$$

where Z is the normalization factor, $C = \{C_1, C_2, ..., C_P\}$ is the set of all cliques in the graph, ψ_c is a potential function defined on the variables (X_c, Y_c) in clique C_p, and θ_p is a set of parameters of the model [42]. We can represent undirected graphical models by a factor graph, where a factor node is there for each potential function and connects to every node in its clique, as shown in Figure 2. Usually, there are two types of potential functions in CRFs: (1) association potential that equals the local conditional distribution over observations $p(Y_c|X_c)$ and (2) interaction potential that encodes the dependency between different output variables. Although both of them are originally defined as Gibbs distribution on features in [37], unary association potentials are often substituted by supervised discriminant classifiers such as neural networks [38] [43].

As for inference on the CRFs, any method for undirected graphical models can be applied, and one of these methods is Belief Propagation (BP) [44]. There are two types of BP algorithms: sum-product and max-sum. They are exact inference methods, respectively, for finding marginal probability and maximizing posterior probability on tree-like graphical models. But because they only involve local message updates, they can also be applied to graphs with loops, resulting in Loopy Belief Propagation. Although Loopy Belief Propagation is not guaranteed to converge, it has achieved success in a variety of domains [45] [46] [47]. It has also been shown that the result of Loopy Belief Propagation corresponds to the stationary point of Bethe free energy and that it is related to variational methods [48]. Readers are referred to [49] for further information on CRFs and Loopy Belief Propagation.

III. Face Datasets

We leverage the CASIA-Webface [7], and VGG-Face [8] datasets to train networks for finding the representation to be used for clustering. We then evaluate performance of our clustering algorithm on two benchmarks datasets, LFW [3], and IARPA Janus Benchmark-B (IJB-B). Some example images from these datasets are shown in Figure 3.

A. LFW

The Labeled Faces in Wild (LFW) [3] contains $13,233$ face images of $5,749$ individuals; of those $5,749$ individuals, $4,069$ have only one face image each. The dataset was constructed by searching for images of celebrities and public figures, and retaining only those images for which an automatically detectable face via the off-the-shelf face detectors [6] was present. As a result, facial pose variations in LFW are limited.

B. IJB-B

The IJB-B dataset [4] is composed of 7 different experiments, with increasing number of subjects. These experiments, respectively, involve 32, 64, 128, 256, 512, $1,024$, $1,870$ subjects with total of $1,473$, $2,566$, $4,793$, $11,186$, $19,583$, $37,653$ and $68,714$ images, respectively. Two protocols related to clustering are defined for IJB-B dataset: (i) clustering of detected faces and (ii) face detection + clustering. Since the focus of this work is face clustering, we will use the first protocol and assume faces have already been detected. The faces are aligned following the procedure in [50], using the bounding boxes provided in IJB-B as the starting point for landmark detection. Many images in the IJB-B datasets are in extreme poses or of low quality, making the clustering task more difficult for IJB-B than for LFW.

C. CASIA-Webface

The CASIA-webface dataset [7] is a semi-automatically collected face dataset for pushing the development of face recognition systems. It contains $494,414$ images of $10,575$ subjects (mostly celebrities) downloaded from internet. However, we are unable to localize faces in some of the images with the face detector in Dlib library [2]. So we use a subset of CASIA-Webface with $404,992$ face images $10,533$ subjects to train our network. This dataset has been popular for training deep networks.

[2] http://dlib.net

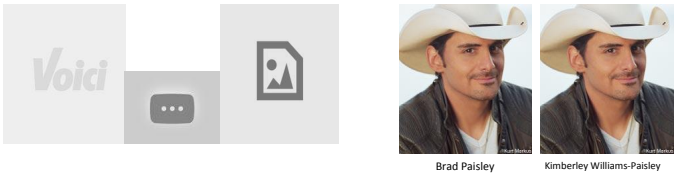

(a) (b)

Fig. 4: Two types of unlabeled duplicate files in VGG-Face. (a) placeholder images, served by some image hosts in place of broken links, and (b) exact duplicates of an image uploaded to two different URLs, labeled as two different subjects "Brad Paisley" and "Kimberley Williams-Paisley".

D. VGG-Face

The VGG-Face dataset was released in 2016 as a set of 2.6 million URLs with corresponding face detection locations [8]. We could acquire only 2.2 million images of the original 2.6 million listed URLs due to broken links. Example VGG images are shown in Figure 3(d).

Some URLs were listed multiple times in VGG-Face, with different subject labels. On manual examination, we found these repeatedly listed URLs were often mislabeled, so we removed them from the dataset. This reduced the number of available images to 1.9 million. However, even after eliminating repeatedly listed URLs, we found that there were still some exact duplicate images as shown in Figure 4, deleting these left us with a total of 1.7 million images. Manually examining the images of random subjects also typically revealed a number of mislabeled images, as in Figure 5. This suggests that manually pruning the training set, or incorporating some form of tolerance to label errors could improve our face representation.

Table I shows the number of images available for use as a training set, under the restrictions mentioned above. We also considered combining the VGG-Face dataset with the CASIA-Webface dataset for network training. However, there is a substantial overlap in subjects between these two datasets; of the $2,622$ subjects in VGG, $1,871$ are also subjects in the CASIA-Webface dataset, leading to a total of just $11,326$ unique subjects in the combined dataset.

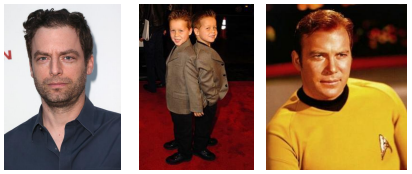

Fig. 5: Three images, labeled as "Justin Kirk." The leftmost image is the actor in question, the middle image contains some incorrectly labeled children, and the rightmost image is the fictional character "James Kirk," played by William Shatner.

TABLE I: Number of images and subjects available for training.

Dataset	# of Images	# of subjects
VGG-Full Dataset	2.62M	$2,622$
VGG-No Duplicate URLs	2.3M	$2,622$
VGG-No Duplicate URLs & Downloadable Images	1.9M	$2,622$
VGG-No Duplicate Files & Downloadable Images	1.7M	$2,622$
CASIA-Webface	$494,414$	$10,575$
CASIA-Webface, with Faces Detected	$435,487$	$10,575$
VGG-No Duplicate Files & CASIA-Webface, with Faces Detected	2.1M	$11,326$

IV. Methods

A. Face Representation: Deep Residual Networks

He et al. [9] used a "deep residual network" architecture to achieve state-of-the-art results on the ImageNet object recognition dataset. The basic observation of He et al. is that when adding layers to a conventional CNN, there comes a point when further addition of layers neither improves training accuracy nor the accuracy on the independent test set. So rather than the typical over-fitting problem (where an overly complex model fits the training set well, but fails to generalize), the observed issue is an underfitting problem, where the optimization procedure fails to fit the more complex model to the training set in the first place.

Due to the incorporation of batch normalization layers [51], the authors argue that the difficulty of optimization problem is not due to numerical computation of gradients, but rather is related to the difficultly in learning an identity mapping with a conventional network architecture. Given a convolutional layer, and activation layer, it is theoretically possible to learn a set of weights that passes through the input unchanged, but in practice this seems difficult to achieve during optimization. This is directly relevant to the underfitting issue discussed earlier in that it should always be possible to stack more layers without hurting training set accuracy, as long as the layers can converge to an identity mapping.

The proposed solution is the residual network block [52]. The basic idea is that rather than learning a direct mapping of the input, the network learns an intermediate representation which is added to the input (a residual), at each block. This is accomplished through the use of a "skip" connection, where the input to residual block x is passed through a series of convolutional layers in one branch, but also passed directly through without alteration in another branch, with both branches being combined in a simple addition operation, and pass the result through a ReLU layer. He et al. [52] proposed a further modification where the block is slightly restructured to remove the final ReLU layer out of the skip connection, reducing the distortion of the output before entering the next residual block.

We directly adapt the proposed architecture for face recognition (leveraging the Torch7 framework[3] and the implementation of residual networks released by Facebook AI Research fb.resnet.torch[4]). We have investigated the 18, 50, and 101-layer architectures outlined in [9]. In terms of data augmentation, we scale our normalized face images following the alignment procedure proposed in [50] to 256×256, as shown in Figure 6, and randomly crop 224×224 regions during training. We additionally flip images during training, and use the scale and aspect-ratio augmentations from [53].

B. Clustering Method

1) Problem Formulation: Given a dataset X of size N, where each $X_i, i = 1, 2, ...N$ is a data point, we want to

[3]http://torch.ch/

[4]https://github.com/facebook/fb.resnet.torch

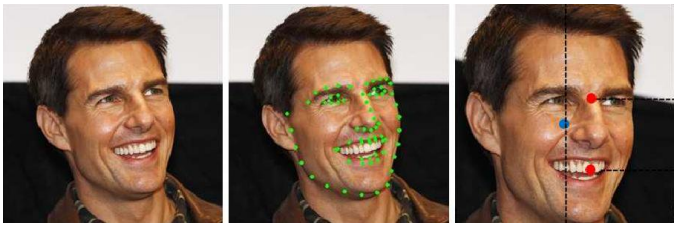

Fig. 6: An example for normalizing the images. We normalize all our images before feeding into the network according to the procedure in [50], where the figure is taken from.

directly estimate an $N \times N$ adjacency matrix Y, where Y_{ij} is a binary variable indicating whether X_i and X_j are assigned to the same cluster. Assuming that we are given the pairwise conditional probability $p(Y_{ij}|X_i, X_j)$ for all pairs, we now want to find the overall adjacency matrix Y maximizing the posterior probability $p(Y|X)$. To model this conditional distribution, we need to consider the dependency between different variables Y_{ij}, for which we propose a triplet interaction constraint to constrain the adjacency matrix Y to be *valid*. By *valid*, we mean that the corresponding graph of that adjacency matrix is transitive and represents a valid partition.

This leads to a structured prediction problem, so we use a Conditional Random Field (CRF) model to formulate it and maximize the posterior probability:

$$p(Y|X) = \frac{1}{Z} \prod_{i<j} \psi_u(Y_{ij}) \prod_{i<j<k} \psi_t(Y_{ij}, Y_{ik}, Y_{jk}), \quad (2)$$

where Z is the normalizing factor, the unary association potential $\psi_u(Y_{ij}) = p(Y_{ij}|X_i, X_j)$ is the pairwise conditional distribution over observations and $\psi_t(Y_{ij}, Y_{ik}, Y_{jk})$ is the triplet interaction potential to constrain Y to be valid. Because the adjacency matrix is symmetric, we only need to take Y_{ij} with $i < j$ as variables, so there are in all $\frac{1}{2}N(N-1)$ output nodes. Notice that the unary potential is the likelihood of a pair of data points belonging to the same class, which is exactly what the pairwise similarity stands for, so we apply a transformation to the cosine similarity between the deep representations of two faces to attain the genuine unary potential $\psi_u(Y_{ij} = 1)$. In practice, we find that this works well, even without attempting to explicitly model the probability distribution for unary potential.

For a partitional clustering, if a point i is connected to any point j in a cluster, it should also connect to all the other points in that cluster but not to any point outside the cluster. However, not every adjacency matrix satisfies this requirement. In order to check the validity of an adjacency matrix, we use a measure based on triplet consistency. Consider a triplet of any three points, as shown in Figure 7. Then there are four possible cases regarding the states of three pairs in one triplet. An adjacency matrix is valid if and only if none of the triplets is in case (2). Hence we can model the dependency between different Y_{ij} with triplet cliques. In our undirected graph, every triplet (Y_{ij}, Y_{ik}, Y_{jk}) is fully connected, and forms a clique. The interaction potential for a triplet clique is defined as:

$$\psi_t(Y_{ij}, Y_{ik}, Y_{jk}) = \exp\left(-\alpha V(Y_{ij}, Y_{ik}, Y_{jk})\right), \quad (3)$$

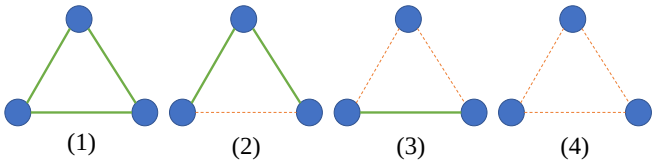

Fig. 7: Four cases of pairwise adjacency in a triplet. A green line means the two points are connected, i.e. assigned to the same cluster. And a red dash line means the two points are not connected. A valid partition is obtained if and only if none of the triplets are in case (2).

where the energy function V is an indicator function which is 1 *iff* the triplet is inconsistent and 0, otherwise:

$$\begin{aligned} V(Y_{ij}, Y_{ik}, Y_{jk}) =& (1 - Y_{ij})Y_{ik}Y_{jk} + Y_{ij}(1 - Y_{ik})Y_{jk} \\ &+ Y_{ij}Y_{ik}(1 - Y_{jk}) \end{aligned} \quad (4)$$

Because the potentials are multiplied in the posterior probability, if α in Equation 3 is sufficiently large such that it dominates the formula, the optimal solution has to be a valid clustering, making this a hard constraint. However, it is worth noting here that we don't need to explicitly define α in our algorithm, as shown in the next subsection.

Due to numerical issues, usually we take the negative logarithm on both sides of Equation 2 and minimize its corresponding energy function:

$$E(Y, X) = \sum_{i<j} D(Y_{ij}) + \sum_{i<j<k} \alpha V(Y_{ij}, Y_{ik}, Y_{jk}), \quad (5)$$

where $D(Y_{ij}) = -\log \psi_u(Y_{ij})$ is the unary potential energy.

The graph structure of the model is illustrated in Figure 8. Each output node Y_{ij} is in N cliques: one pairwise clique with input pair X_i and X_j, and $N-1$ triplet cliques consisting of Y_{ij}, Y_{ik} and Y_{jk}.

2) Inference By Belief Propagation: With the factor graph and potentials defined, we can derive a message formula based on the max-product algorithm. Because we are minimizing energy instead of maximizing probability, the max-product algorithm becomes a min-sum algorithm. We define a message $a_{ij}(Y_{ij})$ as a function of variable Y_{ij}, representing the accumulated energy so far for each state of the variable Y_{ij}. The main procedure of our algorithm is as follows:

1. Initialize all messages as:

$$a^0_{ij}(Y_{ij}) = D(Y_{ij}), \quad (6)$$

which is actually the message sent from the unary potential factor.

2. At iteration $t = 1, 2, ...T$, update the messages as:

$$\begin{aligned} a^t_{ij}(Y_{ij}) = \sum_{k \in N^{t-1}(i,j)} & \min_{Y_{ik}, Y_{jk}} a^{t-1}_{ik}(Y_{ik}) + a^{t-1}_{jk}(Y_{jk}) \\ & + \alpha V(Y_{ij}, Y_{ik}, Y_{jk}), \end{aligned} \quad (7)$$

where we are summing up the messages from different factors.

3. The final state of the variable is determined by:

$$Y_{ij} = \arg\min_{Y_{ij}} a^T_{ij}(Y_{ij}), \quad (8)$$

Here, $N^{t-1}(i, j)$ means the set of the points (not nodes) that are adjacent to either i or j at $(t-1)$ iteration, where by adjacent we mean it has a less positive energy than the

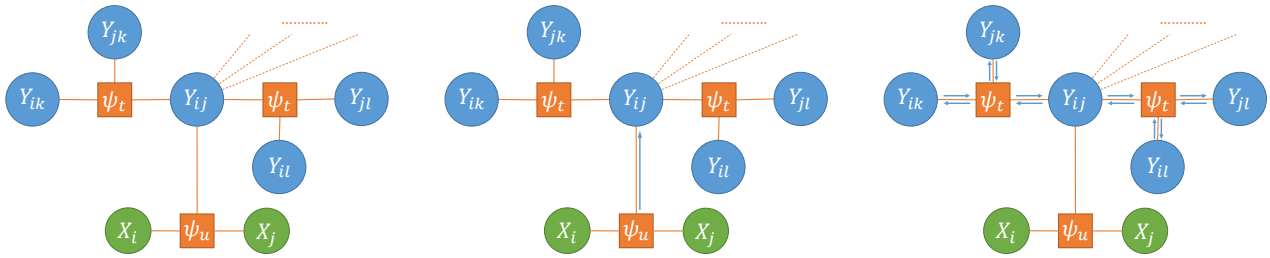

(a) Factor graph (b) Initialization (c) Iteration

Fig. 8: A graphical illustration of the proposed Conditional Random Field using the neighborhood of output node Y_{ij} as an example. The figure shows how the nodes are connected, how the factors are related to potentials and how the messages are passed in the graph. Each green node is an input node corresponding to one data point, each blue node is an output node corresponding to an element in the adjacency matrix, and each rectangle is a factor node representing a potential function, which encodes the constraint between variables. The dash lines represents the omitted links in this figure. There are two kinds of constraints: (i) unary potential which pushes the output to conform with the pairwise similarity and (ii) interaction potential which forces output nodes to be consistent so that Y is valid. During the optimization, messages are propagated among output nodes to directly approach a valid adjacency matrix Y which best retain the similarity information.

negative one in that iteration. If there are still inconsistent triplets after the third step, a transitive merge is applied to ensure the clustering result Y is valid. There are several issues worth discussing on this procedure:

First, this is not a standard Loopy Belief Propagation algorithm for CRF in two ways: (1) the unary messages are sent only once and (2) the messages are isotropic, i.e. a message sent from a node Y_{ij} is the sum of all messages it receives. We found that these modifications make the algorithm easier to implement, use less memory, result in faster convergence and avoid oscillation with little impact on the quality of the results.

Second, the messages could be normalized by subtracting the same value on both sides. Theoretically, it makes no difference to the result, but could avoid numerical underflow and provide stability.

Third, the received messages in Equation 7 only include those neighbors k that are adjacent to at least one of i and j in the last iteration, because the messages from other neighbors would have the same value in both dimensions. Thus it makes no difference if we ignore those $k \notin N^{t-1}(i,j)$. For the same reason, we only need to update Y_{ij} whose $N^{t-1}(i,j)$ is not empty.

Fourth, as we assume that α is a very large number, actually all of the cases where $V(Y_{ij}, Y_{ik}, Y_{jk}) = 1$ could be ignored when we are taking the minimum in equation (7). For example, for $Y_{ij} = 1$, we don't need to consider the cases where $Y_{ik} = 0, Y_{jk} = 1$ or $Y_{ik} = 1$ and $Y_{jk} = 0$. In all the other cases, because $V(Y_{ij}, Y_{ik}, Y_{jk}) = 0$, α disappears from the formula.

Given the above optimization, along with our use of adjacency lists and an update list, the complexity of the algorithm is $O(TNM^2)$, where N is the number of data points, T is the number of iterations, and M is the maximum degree[5] of any data point in any iteration. Furthermore, we only choose to update the nodes that are in at least one inconsistent triplet, so the update list is typically much shorter after several iterations. On the LFW dataset, only 0.59% of the total pairs[6] are updated, and no more than $1,000$ pairs are in the update list after the fourth iteration.

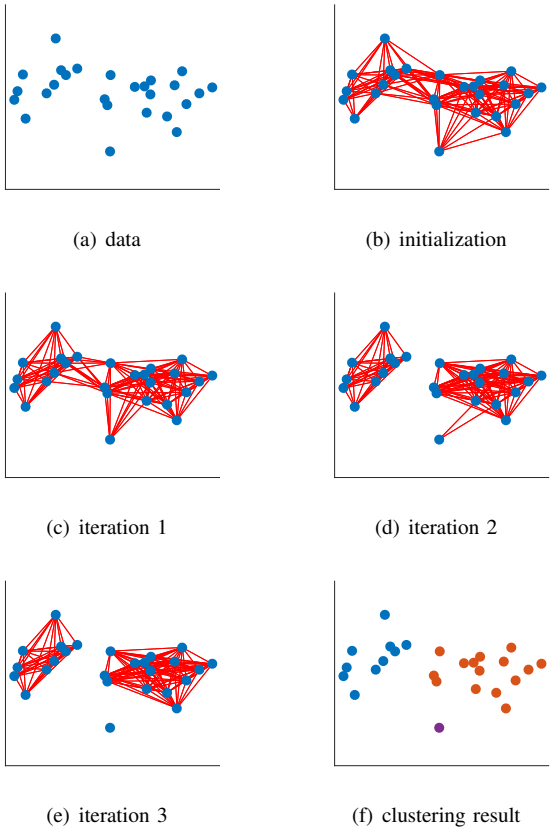

(a) data (b) initialization (c) iteration 1 (d) iteration 2 (e) iteration 3 (f) clustering result

Fig. 9: The proposed clustering procedure on a toy example generated by a mixture of two Gaussian distributions. Gaussian kernel is used as the transformation function to give the unary potential.

An illustration of the complete clustering algorithm on a toy example with synthetic 2-dimensional data is shown in Figure 9. Figure 9(a) shows the initial data points without

[5]Number of adjacent points.

[6]There are in all $87,549,528$ pairs in the LFW dataset.

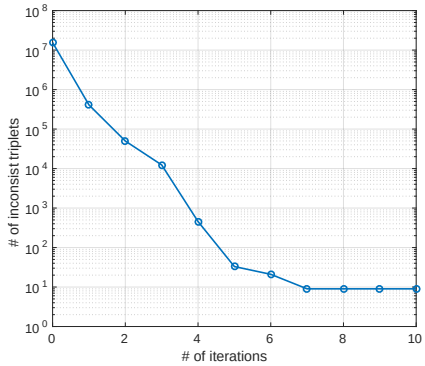

Fig. 10: Number of inconsistent triplets decreases rapidly until convergence.

labels. Figure 9(b) shows the estimated positive pairs based on unary potential ($\psi_u(Y_{ij}=1) >= \psi_u(Y_{ij}=0)$). Figures 9(b)-(d) show the pairs that are adjacent during the first three iterations. The triplet energy becomes zero after the third iteration and so the algorithm converges. Figure 9(f) shows the clustering result. Notice that we did not specify the number of clusters, instead the algorithm dynamically finds them according to the initial similarity and a threshold provided by the user as hyperparameter. Our algorithm is also able to find outliers, shown in this example as a singleton cluster.

Figure 10 shows how the number of inconsistent triplets decreases with iterations during clustering of the $13,233$ images in the LFW dataset. The model converges rather quickly to a stage where only a small number of inconsistent triplets remain. Because the number of remaining inconsistent triplets is usually very small, we don't explicitly force convergence to 0 but apply a transitive merge on the current adjacency matrix to get the final valid clustering. On LFW, only 6 pairs change their states after we apply transitive merge.

3) Semi-supervised clustering: In semi-supervised or constrained clustering, we utilize the given side information, usually in the form of "must-link" pairs and "cannot-link" pairs. These pairs can either be specified by users or automatically generated with another algorithm to improve clustering performance. One way to make use of these pairs is to propagate the constraints. Because our framework is optimized by propagating messages, it becomes quite straight forward to incorporate these constraints: we change the unary potential of the constrained pairs based on the side information provided. If we are very confident with the given constraints (as is the case in our experiments which use ground-truth labels for side information), we can set them as the positive unary potential as 1 for must-link and 0 for cannot-link constraints, resulting in very large unary energy for one state and zero for the other. Equation (7) states that very high energy would be avoided when passing messages so the model can still be optimized under these constraints.

4) Efficient Variant of the clustering algorithm using k-NN Graph: The complexity of the proposed clustering algorithm depends on the degree of data points during the optimization. However, since this number is not fixed, in the worst case its complexity could still be close to $O(TN^3)$, where T and N are the number of iterations and data points, respectively.

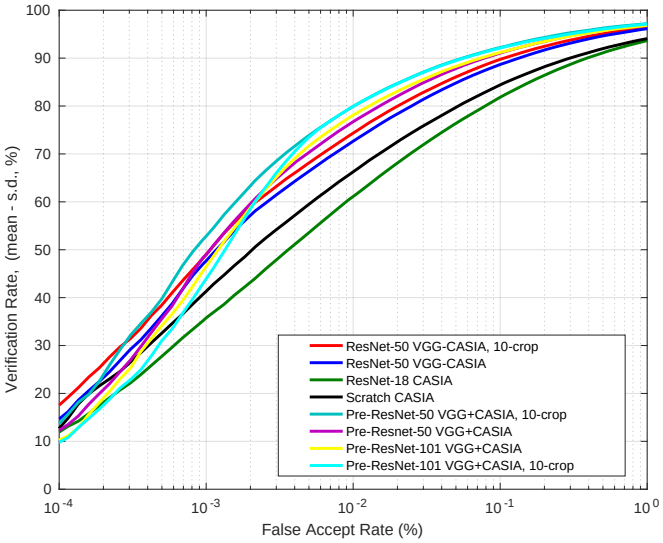

Fig. 11: ROC Curves for the LFW dataset under the BLUFR protocol. Different plots correspond to different networks trained on different datasets. While these results are for a verification problem, they help us in our choice of face representation for clustering

Therefore, we propose a variant of the algorithm which has a fixed linear complexity. The idea is similar to the one in [2], which takes advantage of approximate k-NN methods. Instead of estimating the adjacency of every pair within the dataset, we optimize the joint posterior probability of all Y_{ij} in the k-NN graph which is a subset of the elements in the full adjacency matrix Y. The same procedure outlined in section IV-B2 can still be used for optimization with a few modifications: (1) The neighbor list $N(i)$ now is a fixed list given by the approximate k-NN method, (2) we only update Y_{ij} where $i \in N(j)$ or $j \in N(i)$, and (3) we only need to compute the unary potential in the initialization step for pairs which will be used in the next iteration, i.e. they are neighbors or they have at least one shared neighbor. While time complexity of this variant, given a pre-computed k-NN graph, is also $O(TNM^2)$ as in section IV-B2, M is now a fixed number, which means the algorithm has linear complexity in N per iteration. In particular, we use the same approximate k-NN method, k-d tree, with same configuration as in [2].

V. Experimental Results

A. Face Representation Performance

Our ResNet model is trained on different training sets. The corresponding verification results on the LFW dataset under BLUFR protocol are shown in Table II. Results from [50] are used as the baseline in (Table II, rows 1 and 2). As a proof of concept, we first trained an 18-layer residual network on the CASIA-Webface dataset (Table II, row 3), and attained verification results a bit worse than the baseline [50]. This is expected, since in the original ResNet paper, 18-layer networks showed no substantial improvement over their VGG-style counterparts. Next, we attempted to train a 50-layer residual network, using the full VGG-Face dataset. This was ultimately not very effective, as the optimization stalled and attained worse performance on BLUFR than we attained with a smaller

TABLE II: BLUFR verification performance on LFW using different network architectures and training sets. Results reported as (mean - standard deviation) across 10 folds.

	Training Set	Network	VR@FAR=0.1%
(1)	CASIA-Webface	From Scratch [50]	84.41%
(2)	CASIA-Webface	From Scratch [50], fusion of 9 models	88.00%
(3)	CASIA-Webface	18-layer ResNet	82.06%
(4)	VGG-CASIA	50-layer ResNet	88.67%
(5)	VGG-CASIA	50-layer ResNet, 10-crop	89.74%
(6)	CASIA-Webface	50-Layer Pre-ResNet	88.36%
(7)	CASIA-Webface	50-Layer Pre-ResNet, 10-crop	89.64%
(8)	VGG-Face	50-Layer Resnet	81.40%
(9)	VGG-Deduplicated	50-Layer Pre-ResNet	86.98%
(10)	VGG-Deduplicated+CASIA-Webface	50-Layer Pre-ResNet	91.04%
(11)	VGG-Deduplicated+CASIA-Webface	50-Layer Pre-ResNet, 10-crop	92.22%
(12)	VGG-Deduplicated+CASIA-Webface	101-Layer Pre-ResNet	91.18%
(13)	VGG-Deduplicated+CASIA-Webface	101-Layer Pre-ResNet, 10-crop	92.10%

network trained on the CASIA-Webface dataset (Table II, row 8). We then re-trained this 50-layer architecture on the CASIA-Webface dataset, for 37 epochs, and attained notably better performance than our prior results on the BLUFR benchmark (Table II, row 4).

Due to the substantial amount of time spent retraining on the CASIA-Webface dataset, it is natural to wonder if the initial training on VGG had any significant effect. We therefore trained a 50-layer network solely on CASIA-Webface (this time using the fully pre-activated network variant discussed in [52]), and attained slightly worse results (Table II, row 6). However, the difference between the network's performance was less than 1 standard deviation, so it is difficult to credit this as a significant difference, and it seems that training on the VGG-Face dataset initially lead to no significant improvement.

Subsequently, we attempted to train a network on the deduplicated VGG-Face dataset (removing all images involved in duplicate URL sets, and all images with exact file duplicates). This improved performance over training on the full VGG-Face dataset (Table II, row 9), but the results still lag behind the network trained on CASIA-Webface. Training on the combination of the CASIA-Webface and deduplicated VGG-Face datasets did improve our verification rate at 0.1% FAR to 92.22% (Table II, row 11) from our previous best result of 89.74% (Table II, row 5). We additionally trained a 101-layer network on the combined VGG-Face and CASIA-Webface dataset; however, although this reduced our observed error on the validation set (consisting of a random sample of images of the training set subjects), it did not lead to improved performance on BLUFR, as shown in Table II, row 13.

The best results we have attained on BLUFR is 92.22% VR at 0.1% FAR for verification, and 62.05% DIR at 1% FAR for open-set identification slightly. These lag some newly reported results on the protocol. For example, Cheng at al. [54] used a GoogLeNet-style inception architecture combined with traditional Joint-Bayes and attained a 92.19% VR at 0.1% FAR. They further improved this result to 93.05% using their method for estimating the Joint-Bayes parameters. Lv et al. [55] proposed a data augmentation method (perturbing detected facial landmark locations, prior to image alignment), again using an Inception architecture, and attained a 63.73% DIR at 1% FAR in open-set identification, using the fusion of 3 models (the best single-model performance is 57.90%). These results indicate that our results could potentially be further improved, through the incorporation of metric learning methods, or fusing multiple models.

Figure 11 shows ROC curves for the networks and training set mentioned above on the BLUFR protocol. The main observations based on Figure 11 are as follows:

- The 50-layer ResNet leads to a significant improvement compared to the baseline [50].
- using the standard ImageNet 10-crop strategy (Table II, row 5,7,11,13), leads to a minor improvement in verification performance.
- On the standard LFW protocol, we attain (1-EER)% error of 97.23.

B. Face Clustering

With the representation from our best network architecture (Table II, row 11), we evaluate our clustering algorithm on two unconstrained face datasets (LFW and IJB-B). Before applying the message passing procedure, we obtain unary potentials described in IV-B and shown in Figure 12. Threshold τ is the only parameter throughout our experiments. Different τ provide different prior knowledge and controls the clustering result. But it is worth emphasizing that the transformation function itself (Figure 12) is not a necessary part of the clustering algorithm and neither is the parameter τ, if we could obtain the expected pairwise conditional probabilities in other ways. All the clustering results reported here are based on $\tau = 0.7$.

We call our algorithm as Conditional Pairwise Clustering (ConPaC) which is implemented in C++ and evaluated on Intel Xeon CPU clocked at 2.90GHz using 24 cores. ConPac algorithm is compared to the following benchmarks: (1) K-means, (2) Spectral Clustering [56], (3) Rank-order clustering [26], and (4) Approx. Rank-order clustering [2]. We use the MATLAB R2016a implementation of K-means algorithm and a third-party MATLAB implementation of Spectral Clustering[7]. We use the same representation and cosine similarity for K-means and Spectral Clustering and Rank-order algorithms, but for Approx. Rank-order, we followed [2] because it generated better clustering results.

[7]http://www.mathworks.com/matlabcentral/fileexchange/34412-fast-and-efficient-spectral-clustering/content/files/SpectralClustering.m

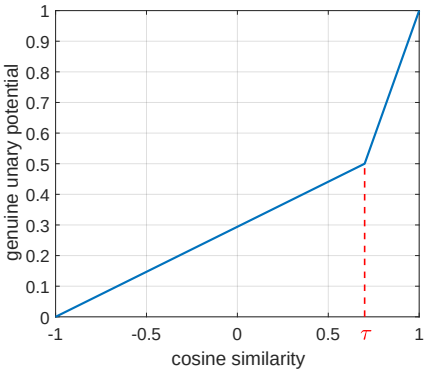

Fig. 12: Transformation function to map the cosine similarity to the genuine unary probability $\psi_u(Y_{ij} = 1)$. A threshold τ is used to split the function into two pieces.

1) Evaluation Measures: Two measures are used to evaluate the clustering results, *Pairwise F-measure* and *BCubed F-measure*. Both compute a *F-score*, which is the harmonic mean of *Precision* and *Recall*. The difference between them lies in the metrics used for precision and recall.

In *Pairwise F-measure*, *Precision* is defined as the fraction of pairs that are correctly clustered together over the total number of pairs that belong to the same class. *Recall* is defined as the fraction of pairs that are correctly clustered together over the total number of pairs that are in the same cluster. In other words, we are using the labels for all the $\frac{1}{2}N(N-1)$ pairs in the dataset with N points. Thus, we can define the True Positive Pairs (TP), False Positive Pairs (FP) and False Negative Pairs(FN). Then *Precision* and *Recall* can be calculated as:

$$Pairwise\ Precision = \frac{TP}{TP + FP} \tag{9}$$

$$Pairwise\ Recall = \frac{TP}{TP + FN} \tag{10}$$

BCubed F-measure [57] defines *Precision* as point precision, namely how many points in the same cluster belong to its class. Similarly, point recall represents how many points from its class appear in its cluster. Formally, we use $L(i)$ and $C(i)$ to, respectively, denote the class and cluster of a point i, and define the *Correctness* between two points i and j as:

$$Correctness(i,j) = \begin{cases} 1, & \text{if } L(i) = L(j) \text{ and } C(i) = C(j) \\ 0, & \text{if otherwise} \end{cases} \tag{11}$$

The *Precision* and *Recall* are defined as:

$$BCubed\ Precision = \text{Avg}_i[\text{Avg}_{j \in C(i)}[Correctness(i,j)]] \tag{12}$$

$$BCubed\ Recall = \text{Avg}_i[\text{Avg}_{j \in L(i)}[Correctness(i,j)]] \tag{13}$$

The F-measure, or F-score for both criteria is given by:

$$F = \frac{2 \times Precision \times Recall}{Precision + Recall} \tag{14}$$

Pairwise F-measure is a more commonly used measure, and *BCbued F-measure* is the formal evaluation measure for the IJB-B dataset. The difference between the two is that *Pairwise F-measure* puts relatively more emphasis on large clusters because the number of pairs grows quadratically with cluster size, while under *BCubed F-measure* clusters are weighted linearly based on their size.

TABLE III: Comparison of the F-measures of the proposed algorithm and other clustering algorithms on LFW dataset. The number of identities (true number of clusters) in LFW is $5,749$. Run-time is reported in the format of hh:mm:ss.

Algorithm	Pairwise F-measure	BCubed F-measure	# of Clusters	Run-time
K-means	0.098	0.680	5,749	00 : 04 : 08
K-means	0.359	0.460	500	00 : 00 : 14
Spectral	0.033	0.559	5,749	01 : 00 : 56
Spectral	0.257	0.249	75	14 : 37 : 14
Rank-Order	0.813	0.891	5,699	00 : 00 : 33
Approx. Rank-Order	0.861	0.875	6,801	00 : 00 : 12
ConPaC (proposed)	0.965	0.922	6,352	00 : 00 : 39

2) Evaluation on the LFW Dataset: LFW is quite an imbalanced dataset, with only 1,680 classes (individuals) containing more than one faces. Since we cannot assume that our datasets will be well balanced, we do the experiments on the whole LFW dataset.

The number of clusters C is dynamically selected during the update of the ConPaC, but it is required as an input parameter for k-means and spectral clustering. So we first evaluate their performance with the ground-truth or the true number of clusters C, $C = 5,749$. Then we repeat the clustering with several different values and report the one that gives the best performance. Table III shows that the performance of k-means and spectral clustering is poor with the ground-truth C. This is because these two algorithms do not perform well with unbalanced data. Even after tuning C, the proposed algorithm performs significantly better than competing algorithms. For the running time, since the sizes of clusters in the LFW dataset are mostly very small, the time complexity of ConPaC is low and it take less than one minute to finish.

Some example clusters by ConPaC results for LFW are shown in Figure 13, where 13(a) and 13(b) show two pure clusters while 13(c) and 13(d) show two impure clusters. Face images in these clusters have different illumination, background, and pose. In 13(c) three images from one identity and 5 from another are grouped together. In 13(d), a total of 6 images from two different identities are grouped into one cluster.

3) Evaluation on the IJB-B Dataset: The results of the 7 experiments in the IJB-B clustering protocol are shown in Table IV. As expected, as the number of identities increases, the F-scores of both competing and the proposed algorithms decrease. While the proposed algorithm shows a larger advantage in terms of F-score on the first few experiments, the gain diminishes as the number of clusters increase. As explained in Section V-B6, this decrease in performance is mainly due to the saliency of the representation.

Another thing worth noticing is that the number of clusters found by the proposed algorithm is much larger than the true number of clusters. This is because a large number of points are regarded as outliers by our algorithm and so they form singleton clusters. For this reason, we also report the number of "non-singleton" clusters in parentheses, which contain at

Fig. 13: Example clusters by the proposed clustering algorithm on LFW datasets.

Fig. 14: Example clusters by the proposed clustering algorithm on IJB-B datasets, (a) and (b) are example clusters from the IJB-B-32 experiment and (c) and (d) are example clusters from IJB-B-1024 experiment.

least two points. The number of non-singleton clusters is closer to the true number of clusters.

Some example clustering results on the IJB-B-32 and IJB-B-1024 are shown in Figure 14. Figure 14(a) and Figure 14(b), respectively, show a pure and an impure cluster on IJB-B-32. Figure 14(c) and Figure 14(d), respectively, show a pure and impure cluster on IJB-B-1024. The images in Figure 14(b) which have a bounding box of the same color are from the same subject. All images in Figure 14(d) are from different subjects.

4) Semi-supervised Clustering: As we mentioned in Section IV-B3, pairwise constraints could be naturally incorporated into the framework of ConPaC without any modification of the algorithm. Therefore in this section, we assume that we have already been given a set of pairwise constraints and evaluate whether the side-information could improve the clustering performance. We consider two types of constraints:

- *Random Constraints*: must-links and cannot-links are picked randomly from ground-truth positive and negative pairs.
- *Key Constraints*: The similarity between every pair of faces is sorted. Must-links are picked by choosing the positive pairs with the lowest similarity and cannot-links are picked by choosing the negative pairs with highest similarity.

In both cases, we use knowledge of the ground truth identity labels to sample a equal number of must-link and cannot-link constraints. We then test the performance of the algorithm with increasing number of constraints. For random constraints, we run 10 trials and report the average performance. The results are reported in terms of pairwise F-score.

We tested our algorithms in terms of semi-supervised clustering on LFW and IJB-B-1024 dataset. The results of semi-supervised clustering are shown in Figure 15. On LFW, in both cases, the constraints are always helpful to the performance and the more the number of constraints, the larger the improvement in F-score. This is because our algorithm tries to find clustering results that are most consistent with the unary potentials, and when more constraints are provided, the unary potentials can be trusted more. What's more, the number

TABLE IV: Comparison of the F-measures of the proposed algorithms and other clustering algorithm on IJB-B datasets. Numbers of non-singleton clusters in the proposed algorithms are shown in parentheses.

(a) IJB-B-32

Algorithm	Pairwise F-measure	BCubed F-measure	# of Clusters	Run-time
K-means	0.544	0.587	10	00 : 00 : 01
Spectral	0.492	0.570	10	00 : 00 : 01
Rank-Order	0.589	0.628	177	00 : 00 : 02
Approx. Rank-Order	0.706	0.667	262	00 : 00 : 03
ConPaC (proposed)	0.937	0.751	294 (92)	00 : 00 : 09

(b) IJB-B-64

Algorithm	Pairwise F-measure	BCubed F-measure	# of Clusters	Run-time
K-means	0.560	0.510	10	00 : 00 : 01
Spectral	0.303	0.514	25	00 : 00 : 01
Rank-Order	0.366	0.550	410	00 : 00 : 06
Approx. Rank-Order	0.534	0.574	588	00 : 00 : 03
ConPaC (proposed)	0.897	0.656	619 (191)	00 : 00 : 09

(c) IJB-B-128

Algorithm	Pairwise F-measure	BCubed F-measure	# of Clusters	Run-time
K-means	0.488	0.442	25	00 : 00 : 04
Spectral	0.380	0.518	50	00 : 00 : 06
Rank-Order	0.151	0.489	869	00 : 00 : 17
Approx. Rank-Order	0.413	0.482	1,440	00 : 00 : 05
ConPaC (proposed)	0.814	0.563	1,270 (360)	00 : 00 : 14

(d) IJB-B-256

Algorithm	Pairwise F-measure	BCubed F-measure	# of Clusters	Run-time
K-means	0.370	0.377	10	00 : 00 : 13
Spectral	0.243	0.457	75	00 : 00 : 36
Rank-Order	0.346	0.489	4,084	00 : 00 : 16
Approx. Rank-Order	0.401	0.423	3,710	00 : 00 : 12
ConPaC (proposed)	0.459	0.493	2,930 (770)	00 : 01 : 24

(e) IJB-B-512

Algorithm	Pairwise F-measure	BCubed F-measure	# of Clusters	Run-time
K-means	0.329	0.388	100	00 : 00 : 31
Spectral	0.210	0.424	250	00 : 04 : 09
Rank-Order	0.045	0.545	4,084	00 : 03 : 56
Approx. Rank-Order	0.398	0.410	7,010	00 : 00 : 19
ConPaC (proposed)	0.424	0.481	5,677 (1,398)	00 : 03 : 42

(f) IJB-B-1024

Algorithm	Pairwise F-measure	BCubed F-measure	# of Clusters	Run-time
K-means	0.279	0.358	250	00 : 01 : 26
Spectral	0.195	0.392	500	00 : 27 : 21
Rank-Order	0.017	0.417	4,084	00 : 20 : 36
Approx. Rank-Order	0.341	0.352	15,777	00 : 00 : 37
ConPaC (proposed)	0.348	0.452	12,155 (2,804)	00 : 20 : 06

(g) IJB-B-1870

Algorithm	Pairwise F-measure	BCubed F-measure	# of Clusters	Run-time
K-means	0.313	0.398	1000	00 : 06 : 56
Spectral	0.208	0.335	500	01 : 34 : 40
Rank-Order	0.005	0.267	4,084	01 : 12 : 25
Approx. Rank-Order	0.315	0.317	31,218	00 : 00 : 73
ConPaC (proposed)	0.239	0.429	23,119 (5,032)	02 : 53 : 58

of specified constraints in the experiment are actually very small compared with the total number of possible pairwise constraints, which is $(13233 \times 13232) \div 2 = 87,483,363$. But due to message propagation, these constraints impact not only themselves, but also all related pairs. Thus, even a small number of randomly picked constraints could boost the performance significantly. On IJB-B-1024 dataset, the random constraints still help a lot, but the key constraints are not doing any favor. The reason for this could be that because the key constraints are those most in conflict with the cosine similarity matrix, and when the similarity matrix is not very reliable (due to the saliency of the representation), it could be incompatible with the original similarity matrix and lead to poor performance.

5) k-NN variant for large datasets: In this section, we test the run-time and performance of the k-NN variant of the proposed clustering. We use the same k-d tree library [58] as used in [2] to generate the approximate k-NN graph. We also use the same configuration for the k-d tree where $k = 200$ and we build 4 trees with a search size of $2,000$. We first compare the performance of the algorithm using approximate k-NN graph and full graph (original algorithm) on LFW and IJB-B-1024. Then we test the performance of the k-NN variant on 1 million unlabeled face images along with LFW or IJB-B. We apply pairwise F-measure to only the subset for which we have labels (from LFW or IJB-B) but omit those for which we do not have labels (1 million distractor images). Although we don't have the labels for the 1 million dataset, it is still reasonable to apply pairwise F-measure from the view that we are evaluating the label predictions on the adjacency matrix of the subset of dataset. The clustering results is shown in Table V. The proposed k-NN variant perform well on LFW dataset even when there are 1 million distractors, but not well on IJB-B-1024.

6) Influence of the initial similarity matrix: The motivation and distinguishing feature of our algorithm is that it only depends on the given pairwise similarity. In this subsection we want to investigate how the clustering performance is affected by the similarity and also how it is influenced by the choice of parameter.

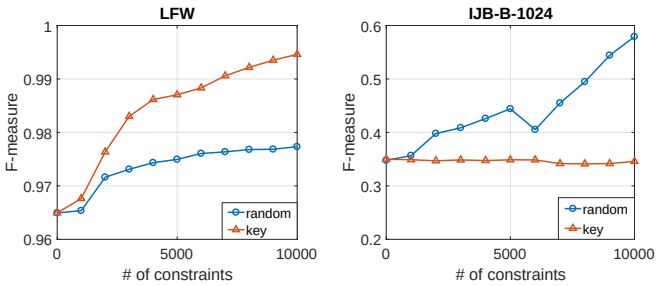

Fig. 15: Performance of the proposed clustering algorithm on LFW and IJB-B-1024 datasets after incorporating pairwise constraints. Both random and key constraints improve clustering performance in terms of F-score on the LFW dataset. However, for the IJB-B-1024 dataset, only random constraints are able to boost the performance.

TABLE V: Performance of k-NN variant and original algorithm on small and large datasets.

Dataset	Version	Pairwise F-measure	# of clusters	Run-time
LFW	full graph	0.965	6,352	00 : 00 : 39
LFW	k-d tree	0.964	5,927	00 : 03 : 06
IJB-B-1024	full graph	0.348	12,155	00 : 20 : 06
IJB-B-1024	k-d tree	0.101	8,352	00 : 05 : 54
1M + LFW	k-d tree	0.809	452,629	04 : 24 : 09
1M + IJB-B-1024	k-d tree	0.061	455,492	04 : 32 : 18

We first need a method to evaluate the reliability of the input pairwise similarity matrix. Notice that with the input similarity matrix and corresponding threshold τ, we can already predict the pairwise connections in the dataset and get a new adjacency matrix Z. Each element Z_{ij} in the matrix Z can be regarded as a prediction result of pairwise verification between two face images based on thresholding the cosine similarity with threshold τ. The difference between Z and Y is that Z is not a valid matrix, so it does not necessarily corresponding to a clustering result. For the toy example in Figure 9, 9(a) is just the corresponding graph of Z and the graph of Y would be 9(b), which is transitive. Though it is not a valid result in terms of clustering, from a label prediction view, we can still apply Equation 9 and Equation 10 to Z and compute the pairwise F-score to measure the input similarity matrix's reliability. Because Z represents the verification results, this reliability can also indicate how good our input similarity is in terms of verification.

We then determine how the F-measures of Y and Z varies with different values of threshold τ in the mapping function. We can see that the clustering performance changes smoothly with different parameter values. Further more, the F-measure of result Y is highly correlated with that of Z. In other words, when the similarity matrix is reliable, the clustering does a better job, and vice versa. Because $\tau = 0.7$ is the best threshold for both LFW and IJB-B-1024, we use it for all the other experiments, as indicated earlier.

To further see the relationship between the clustering performance and the verification performance, we compare the F-measures of Y and that of Z on all the 7 experiments in IJB-B dataset. We find that the two F-measures are almost linearly correlated across all these experiments, with a correlation coefficient of 0.9998. Therefore, we can state that we have achieved our motivation to make full use of the input pairwise similarity, and that the decrease in clustering performance on IJB-B compared to LFW is due to the decrease in reliability of the input pairwise similarity, which in turn depends on the saliency of the face representation (feature vector).

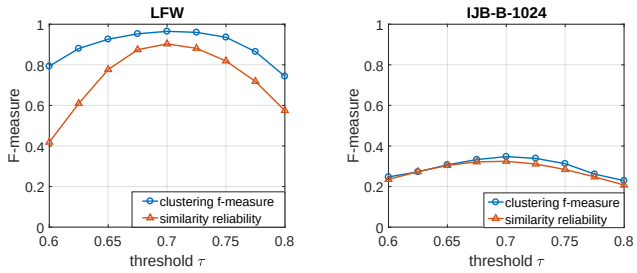

(a) (b)

Fig. 16: Performance of the proposed algorithm with different threshold values on LFW and IJB-B-1024 datasets.

VI. Conclusions

In this paper, we first trained a ResNet deep network architecture on CASIA-Webface and VGG-Face dataset. The representation from the proposed network shows a good performance on the BLUFR face verification benchmark. Using this representation, we proposed a new clustering algorithm, called Conditional Pairwise Clustering (ConPaC), which learns an adjacency matrix directly from the given similarity matrix. The clustering problem is modeled as a structured prediction problem using a Conditional Random Field (CRF) and is inferred by Loopy Belief Propagation. The proposed algorithm outperforms several well known clustering algorithms on LFW and IJB-B unconstrained datasets and it can also naturally incorporate pairwise constraints to improve clustering results. We also propose a k-NN variant of ConPaC which is capable of clustering millions of face images. Our future work would include finding better unary potential for more robust face clustering and also incorporating pairwise constraints into the k-NN variant.

References

[1] J. C. Klontz and A. K. Jain, "A case study of automated face recognition: The Boston Marathon bombings suspects," *IEEE Computer*, vol. 46, no. 11, 2013.

[2] C. Otto, D. Wang, and A. K. Jain, "Clustering millions of faces by identity," *IEEE Trans. on PAMI*, 2017.

[3] G. B. Huang, M. Ramesh, T. Berg, and E. Learned-Miller, "Labeled faces in the wild: A database for studying face recognition in unconstrained environments," University of Massachusetts, Amherst, Tech. Rep. 07-49, October 2007.

[4] C. Whitelam, E. Taborsky, A. Blanton, B. Maze, J. Adams, T. Miller, N. Kalka, A. K. Jain, J. A. Duncan, K. Allen, J. Cheney, and P. Grother, "Iarpa janus benchmark-b face dataset," in *CVPR Workshop on Biometrics*, 2017.

[5] B. F. Klare, B. Klein, E. Taborsky, A. Blanton, J. Cheney, K. Allen, P. Grother, A. Mah, M. Burge, and A. K. Jain, "Pushing the frontiers of unconstrained face detection and recognition: IARPA Janus benchmark A," in *CVPR*, 2015.

[6] P. Viola and M. J. Jones, "Robust real-time face detection," *International Journal of Computer Vision*, vol. 57, no. 2, 2004.

[7] D. Yi, Z. Lei, S. Liao, and S. Z. Li, "Learning face representation from scratch," *arXiv:1411.7923*, 2014.

[8] O. M. Parkhi, A. Vedaldi, and A. Zisserman, "Deep face recognition," in *British Machine Vision Conference*, 2015.

[9] K. He, X. Zhang, S. Ren, and J. Sun, "Deep residual learning for image recognition," in *CVPR*, 2016.

[10] M. Turk and A. Pentland, "Face recognition using eigenfaces," in *CVPR*, 1991.

[11] T. F. Cootes, G. J. Edwards, and C. J. Taylor, "Active appearance models," *IEEE Trans. on PAMI*, vol. 23, no. 6, 2001.

[12] T. Ahonen, A. Hadid, and M. Pietikainen, "Face description with local binary patterns: Application to face recognition," *IEEE Trans. on PAMI*, vol. 28, no. 12, 2006.

[13] J. Wright, A. Y. Yang, A. Ganesh, S. S. Sastry, and Y. Ma, "Robust face recognition via sparse representation," *IEEE Trans. on PAMI*, vol. 31, no. 2, 2009.

[14] A. Krizhevsky, I. Sutskever, and G. E. Hinton, "Imagenet classification with deep convolutional neural networks," in *NIPS*, 2012.

[15] Y. Taigman, M. Yang, M. Ranzato, and L. Wolf, "Deepface: Closing the gap to human-level performance in face verification," in *CVPR*, 2014.

[16] Y. Sun, X. Wang, and X. Tang, "Deep learning face representation from predicting 10,000 classes," in *CVPR*, 2014.

[17] Y. Sun, Y. Chen, X. Wang, and X. Tang, "Deep learning face representation by joint identification-verification," in *NIPS*, 2014.

[18] Y. Sun, X. Wang, and X. Tang, "Deeply learned face representations are sparse, selective, and robust," in *CVPR*, 2015.

[19] Y. Sun, D. Liang, X. Wang, and X. Tang, "Deepid3: Face recognition with very deep neural networks," *arXiv:1502.00873*, 2015.

[20] D. Chen, X. Cao, L. Wang, F. Wen, and J. Sun, "Bayesian face revisited: A joint formulation," in *ECCV*, 2012.

[21] F. Schroff, D. Kalenichenko, and J. Philbin, "Facenet: A unified embedding for face recognition and clustering," in *CVPR*, 2015.

[22] A. K. Jain, "Data clustering: 50 years beyond k-means," *Pattern Recognition Letters*, vol. 31, no. 8, 2010.

[23] J. Ho, M.-H. Yang, J. Lim, K.-C. Lee, and D. Kriegman, "Clustering appearances of objects under varying illumination conditions," in *CVPR*, 2003.

[24] J. Cui, F. Wen, R. Xiao, Y. Tian, and X. Tang, "Easyalbum: an interactive photo annotation system based on face clustering and re-ranking," in *ACM SIGCHI Conference on Human factors in Computing Systems*, 2007.

[25] Y. Tian, W. Liu, R. Xiao, F. Wen, and X. Tang, "A face annotation framework with partial clustering and interactive labeling," in *CVPR*, 2007.

[26] C. Zhu, F. Wen, and J. Sun, "A rank-order distance based clustering algorithm for face tagging," in *CVPR*, 2011.

[27] R. Vidal and P. Favaro, "Low rank subspace clustering (lrsc)," *Pattern Recognition Letters*, vol. 43, 2014.

[28] C. Otto, B. Klare, and A. Jain, "An efficient approach for clustering face images," in *ICB*, 2015.

[29] A. Nech and I. Kemelmacher-Shlizerman, "Level playing field for million scale face recognition," *arXiv:1705.00393*, 2017.

[30] K. Wagstaff, C. Cardie, S. Rogers, S. Schrödl *et al.*, "Constrained k-means clustering with background knowledge," in *ICML*, 2001.

[31] E. P. Xing, A. Y. Ng, M. I. Jordan, and S. Russell, "Distance metric learning with application to clustering with side-information," in *NIPS*, 2002.

[32] S. Basu, M. Bilenko, and R. J. Mooney, "A probabilistic framework for semi-supervised clustering," in *KDD*, 2004.

[33] I. Davidson and S. Ravi, "Agglomerative hierarchical clustering with constraints: Theoretical and empirical results," in *European Conference on Principles of Data Mining and Knowledge Discovery*, 2005.

[34] Z. Lu and M. A. Carreira-Perpinan, "Constrained spectral clustering through affinity propagation," in *CVPR*, 2008.

[35] X. Wang and I. Davidson, "Flexible constrained spectral clustering," in *KDD*, 2010.

[36] S. Basu, I. Davidson, and K. Wagstaff, *Constrained clustering: Advances in Algorithms, Theory, and Applications*. CRC Press, 2008.

[37] J. Lafferty, A. McCallum, F. Pereira *et al.*, "Conditional random fields: Probabilistic models for segmenting and labeling sequence data," in *ICML*, 2001.

[38] X. He, R. S. Zemel, and M. Á. Carreira-Perpiñán, "Multiscale conditional random fields for image labeling," in *CVPR*, 2004.

[39] D. Hoiem, A. A. Efros, and M. Hebert, "Putting objects in perspective," *International Journal of Computer Vision*, vol. 80, no. 1, 2008.

[40] V. Koltun, "Efficient inference in fully connected crfs with gaussian edge potentials," *NIPS*, 2011.

[41] L. R. Rabiner, "A tutorial on hidden markov models and selected applications in speech recognition," *Proceedings of the IEEE*, vol. 77, no. 2, 1989.

[42] C. Sutton and A. McCallum, "An introduction to conditional random fields for relational learning," *Introduction to Statistical Relational Learning*, 2006.

[43] I. K. K. M. Liang-Chieh Chen, George Papandreou and A. L. Yuille, "Semantic image segmentation with deep convolutional nets and fully connected crfs," *ICLR*, 2015.

[44] J. Pearl, *Probabilistic Reasoning in Intelligent Systems: Networks of Plausible Inference*. Morgan Kaufmann, 1988.

[45] W. T. Freeman, E. C. Pasztor, and O. T. Carmichael, "Learning low-level vision," *International Journal of Computer Vision*, vol. 40, no. 1, 2000.

[46] B. J. Frey and D. J. MacKay, "A revolution: Belief propagation in graphs with cycles," *NIPS*, 1998.

[47] C. Yanover and Y. Weiss, *Approximate Inference and Protein-folding*. Hebrew University of Jerusalem, 2002.

[48] J. S. Yedidia, W. T. Freeman, and Y. Weiss, "Constructing free-energy approximations and generalized belief propagation algorithms," *IEEE Transactions on Information Theory*, vol. 51, no. 7, 2005.

[49] C. Sutton, A. McCallum *et al.*, "An introduction to conditional random fields," *Foundations and Trends in Machine Learning*, vol. 4, no. 4, 2012.

[50] D. Wang, C. Otto, and A. K. Jain, "Face search at scale," *IEEE Trans. on PAMI*, 2016.

[51] S. Ioffe and C. Szegedy, "Batch normalization: Accelerating deep network training by reducing internal covariate shift," in *ICML*, 2015.

[52] K. He, X. Zhang, S. Ren, and J. Sun, "Identity mappings in deep residual networks," in *ECCV*, 2016.

[53] C. Szegedy, W. Liu, Y. Jia, P. Sermanet, S. Reed, D. Anguelov, D. Erhan, V. Vanhoucke, and A. Rabinovich, "Going deeper with convolutions," in *CVPR*, 2015.

[54] C. Cheng, J. Xing, Y. Feng, D. Li, and X.-D. Zhou, "Bootstrapping joint bayesian model for robust face verification," in *ICB*, 2016.

[55] J.-J. Lv, C. Cheng, G.-D. Tian, X.-D. Zhou, and X. Zhou, "Landmark perturbation-based data augmentation for unconstrained face recognition," *Signal Processing: Image Communication*, 2016.

[56] A. Y. Ng, M. I. Jordan, Y. Weiss *et al.*, "On spectral clustering: Analysis and an algorithm," in *NIPS*, 2001.

[57] E. Amigó, J. Gonzalo, J. Artiles, and F. Verdejo, "A comparison of extrinsic clustering evaluation metrics based on formal constraints," *Information Retrieval*, vol. 12, no. 4, 2009.

[58] M. Muja and D. G. Lowe, "Scalable nearest neighbor algorithms for high dimensional data," *IEEE Trans. on PAMI*, vol. 36, no. 11, 2014.

Yichun Shi received his B.S degree in the Department of Computer Science and Engineering at Shanghai Jiao Tong University in 2016. He is now working towards the Ph.D. degree in the Department of Computer Science and Engineering at Michigan State University. His research interests include pattern recognition and computer vision.

Charles Otto received his B.S. and Ph.D. degrees in the Department of Computer Science and Engineering at Michigan State University in 2008 and 2016, respectively. He was a research engineer at IBM during 2006-2011. He is currently employed at Noblis, Reston, VA. His research interests include pattern recognition, and computer vision.

Anil K. Jain is a University distinguished professor in the Department of Computer Science and Engineering at Michigan State University. His research interests include pattern recognition and biometric authentication. He served as the editor-in-chief of the IEEE Transactions on Pattern Analysis and Machine Intelligence (1991-1994), a member of the United States Defense Science Board, and and is a member of the National Academy of Engineering.